

# Modeling the Anisotropic Two-Point Galaxy Correlation Function on Small Scales and Single-Probe Measurements of $H(z)$ , $D_A(z)$ , and $f(z)\sigma_8(z)$ from the Sloan Digital Sky Survey DR7 Luminous Red Galaxies

Chia-Hsun Chuang<sup>1\*</sup> and Yun Wang<sup>2</sup>

<sup>1</sup> Instituto de Física Teórica, (UAM/CSIC), Universidad Autónoma de Madrid, Cantoblanco, E-28049 Madrid, Spain

<sup>2</sup> Homer L. Dodge Department of Physics & Astronomy, Univ. of Oklahoma, 440 W Brooks St., Norman, OK 73019, U.S.A.

7 February 2022

## ABSTRACT

We present a simple and efficient phenomenological model for the two-dimensional two-point galaxy correlation function that works well over a wide range of scales, from large scales down to scales as small as  $25 h^{-1}$  Mpc. Our model incorporates nonlinear effects, a scale-dependent galaxy bias on small scales, and allows the redshift-space distortions to be scale and direction dependent. We validate our model using LasDamas mock catalogs, and apply it to the Sloan Digital Sky Survey (SDSS) DR7 Luminous Red Galaxies (LRGs). Using only the monopole and quadrupole of the correlation function measured from the SDSS DR7 LRGs, we obtain improved measurements  $H(z)r_s(z_d)/c = 0.0433 \pm 0.0042$ ,  $D_A(z)/r_s(z_d) = 6.59 \pm 0.46$ , and  $f(z)\sigma_8(z) = 0.429 \pm 0.089$  at  $z = 0.35$ , using the scale range of  $25 < s < 120 h^{-1}$  Mpc. We expect our results and model to be useful in tightening dark energy and gravity constraints from the full analysis of current and future galaxy clustering data.

**Key words:** cosmology: observations, distance scale, large-scale structure of Universe

## 1 INTRODUCTION

In our quest to solve the mystery of the observed cosmic acceleration (Riess et al. 1998; Perlmutter et al. 1999), galaxy clustering plays an increasingly important role as a probe of both dark energy and gravity, the two main classes of possible explanations for cosmic acceleration. Current data from the Sloan Digital Sky Survey (SDSS) Data Release Seven (DR7) (Abazajian et al. 2009), WiggleZ (Blake et al. 2009), and BOSS (Eisenstein et al. 2011) are allowing us to place very useful constraints on dark energy. The planned space mission Euclid<sup>1</sup> will survey  $\sim 60$  million emission-line galaxies at  $0.7 < z < 2$  over 15,000 square degrees (Cimatti et al. 2009; Wang et al. 2010; Laureijs et al. 2011), and provide potentially revolutionary bounds on the nature of cosmic acceleration.

The SDSS data have been analyzed using both the power spectrum method (see, e.g., Tegmark et al. 2004; Hutsi 2005; Padmanabhan et al. 2007; Blake et al. 2007; Percival et al. 2007, 2010; Reid et al. 2010; Montesano et al. 2011), and the correlation function method (see, e.g., Eisenstein et al.

2005; Okumura et al. 2008; Cabre & Gaztanaga 2009; Martinez et al. 2009; Sanchez et al. 2009; Kazin et al. 2010a; Chuang, Wang, & Hemantha 2012; Samushia et al. 2012; Padmanabhan et al. 2012). Although these two methods are simple Fourier transforms of one another, the analysis processes are quite different and the results cannot be converted using Fourier transform directly because of the finite size of the survey volume.

The power of galaxy clustering as a dark energy probe lies in the fact that the Hubble parameter,  $H(z)$ , the angular diameter distance,  $D_A(z)$ , can in principle be extracted simultaneously from data through the measurement of the baryon acoustic oscillation (BAO) scale in the radial and transverse directions (Blake & Glazebrook 2003; Seo & Eisenstein 2003; Wang 2006). The inclusion of information from full galaxy clustering goes beyond BAO only, and enables significantly enhanced constraints on  $H(z)$  and  $D_A(z)$ . Most importantly, it allows the measurement of the growth rate of cosmic large scale structure,  $f(z) = \beta(z)b(z)$  (where  $\beta(z)$  denotes the linear redshift-space distortion (RSD) factor (Kaiser 1987), and  $b(z)$  denotes galaxy bias), required for using galaxy clustering to test gravity (Guzzo et al. 2008; Wang 2008).

In fact, it is possible to measure  $f(z)\sigma_8(z)$  (Song & Percival 2009) or  $f(z)\sigma_m(z)/r_s(z_d)^4$  (Wang 2012) without facing the difficulty of measuring galaxy bias.

\* MultiDark Fellow; E-mail: chia-hsun.chuang@uam.es

<sup>1</sup> <http://www.euclid-emc.org/>

In Chuang & Wang (2012), we made significant improvements in modeling galaxy clustering from previous studies (Okumura et al. 2008; Cabre & Gaztanaga 2009; Kazin et al. 2010b), and succeeded in making the first simultaneous measurements of  $H(z)$  and  $D_A(z)$  from data, using the full 2D correlation function of a sample of SDSS DR7 LRGs (Eisenstein et al. 2001), and without assuming a dark energy model or a flat Universe. Xu et al. (2013) measured  $H(z)$  and  $D_A(z)$  at  $z = 0.35$  from the SDSS DR7 LRGs by applying density-field reconstruction to an anisotropic analysis of the BAO peak. Anderson et al. (2013) applied the same method on SDSS III Baryon Oscillation Spectroscopic Survey (SDSS-III/BOSS) DR9 sample. Regarding the measurements of growth constraints, Samushia et al. (2012) measured  $f(z)\sigma_8(z)$  from SDSS DR7 LRG sample with CMB + SNIa priors. Reid et al. (2012) measured  $H(z)$ ,  $D_A(z)$ , and  $f(z)\sigma_8(z)$  at  $z = 0.57$  from the monopole and quadrupole of the 2D 2PCF of the SDSS-III/BOSS DR9 sample, assuming CMB priors. Most recently, Chuang et al. (2013) applied similar analysis as this paper on SDSS-III/BOSS DR9 sample to measure  $H(z)$ ,  $D_A(z)$ ,  $\Omega_m h^2$  and  $f(z)\sigma_8(z)$  without CMB priors.

In Chuang & Wang (2013), we extended our method by exploring the use of the multipoles of the correlation function to measure  $H(z)$ ,  $D_A(z)$ , and  $\beta(z)$ . The obvious advantage of using multipoles of the correlation function instead of the full 2D correlation function is the reduced number of data points used to obtain similar amount of information.

The proper modeling of RSD is required in order to measure  $\beta(z)$  or  $f(z)$  from galaxy clustering data. Recent work on improving the modeling of RSD include that of Jennings, Baugh, & Pascoli (2011) and Reid & White (2011). In this paper, we focus on the detailed phenomenological modeling of the correlation function on smaller scales to obtain improved constraints on  $\beta(z)$  or  $f(z)\sigma_8(z)$ . We use the multipoles of the 2D correlation function for speed and efficiency.

In Section 2, we introduce the galaxy sample used in our study. In Section 3, we describe the details of our new model. In Section 4, we describe the details of our methodology. In Section 5, we present our improved measurements from SDSS DR7 LRGs. We summarize and conclude in Sec. 6.

## 2 DATA

The SDSS has observed one-quarter of the entire sky and performed a redshift survey of galaxies, quasars and stars in five passbands  $u, g, r, i$ , and  $z$  with a 2.5m telescope (Fukugita et al. 1996; Gunn et al. 1998, 2006). We use the public catalog, the NYU Value-Added Galaxy Catalog (VAGC) (Blanton et al. 2005), derived from the SDSS II final public data release, Data Release 7 (DR7) (Abazajian et al. 2009). We select our LRG sample from the NYU VAGC with the flag *primTarget* bit mask set to 32. K-corrections have been applied to the galaxies with a fiducial model ( $\Lambda$ CDM with  $\Omega_m = 0.3$  and  $h = 1$ ), and the selected galaxies are required to have rest-frame  $g$ -band absolute magnitudes  $-23.2 < M_g < -21.2$  (Blanton & Roweis 2007). The same selection criteria were used in previous papers (Zehavi et al. 2005; Eisenstein et al. 2005; Okumura et al. 2008; Kazin et al. 2010a). The sample we use is referred to as “DR7full” in Kazin et al. (2010a). Our sample includes 87000 LRGs in the redshift range 0.16-0.44.

Spectra cannot be obtained for objects closer than 55 arcsec within a single spectroscopic tile due to the finite size of the fibers.

To correct for these “collisions”, the redshift of an object that failed to be measured would be assigned to be the same as the nearest successfully observed one. Both fiber collision corrections and K-corrections have been made in NYU-VAGC (Blanton et al. 2005). The collision corrections applied here are different from what has been suggested in Zehavi et al. (2005). However, the effect should be small since we are using relatively large scale which are less affected by the collision corrections.

We construct the radial selection function as a cubic spline fit to the observed number density histogram with the width  $\Delta z = 0.01$ . The NYU-VAGC provides the description of the geometry and completeness of the survey in terms of spherical polygons. We adopt it as the angular selection function of our sample. We drop the regions with completeness below 60% to avoid unobserved plates (Zehavi et al. 2005). The Southern Galactic Cap region is also dropped.

## 3 MODELING 2D CORRELATION FUNCTION

In this section, we describe our model which encompasses the linear scale to the nonlinear scale.

### 3.1 Modeling 2D Correlation Function for Large Scales

We compute the linear matter power spectra,  $P_{lin}(k)$ , by using CAMB (Lewis, Challinor, & Lasenby 2000). The linear power spectrum can be composed to two parts:

$$P_{lin}(k) = P_{nw}(k) + P_{BAO}^{lin}(k), \quad (1)$$

where  $P_{nw}(k)$  is the no-wiggle or pure CDM power spectrum calculated using Eq.(29) from Eisenstein & Hu (1998) and  $P_{BAO}^{lin}(k)$  is the wiggled part defined by the equation itself. The nonlinear damping effect of the wiggled part in redshift space can be well approximated by (Eisenstein, Seo, & White 2007)

$$P_{BAO}^{nl}(k, \mu_k) = P_{BAO}^{lin}(k) \cdot \exp\left(-\frac{k^2}{2k_*^2}[1 + \mu_k^2(2f + f^2)]\right), \quad (2)$$

where  $k_*$  could be computed by (Crocco & Scoccimarro 2006; Matsubara 2008)

$$k_* = \left[\frac{1}{3\pi^2} \int P_{lin}(k) dk\right]^{-1/2}. \quad (3)$$

The dewiggled power spectrum is

$$P_{dw}(k, \mu_k) = P_{nw}(k) + P_{BAO}^{nl}(k, \mu_k), \quad (4)$$

$\mu_k$  is the cosine of the angle between  $\mathbf{k}$  and the line of sight (LOS). Note that Eqs.(1)-(4) are the same as Eq.(2) in Chuang & Wang (2012), except for the addition of the direction-dependent terms in the exponent of the damping factor in Eq.(2), but are somewhat more intuitive.

Next, we include the linear RSD as follows to obtain the galaxy power spectrum in redshift space at large scales (Kaiser 1987):

$$P_g^s(k, \mu_k) = b^2(1 + \beta\mu_k^2)^2 P_{dw}(k, \mu_k), \quad (5)$$

$$= P_{g,nw}^s(k, \mu_k) + P_{g,BAO}^s(k, \mu_k), \quad (6)$$

where  $b$  is the linear galaxy bias. Note that we have defined

$$P_{g,nw}^s(k, \mu_k) = b^2(1 + \beta\mu_k^2)^2 P_{nw}(k) \quad (7)$$

$$P_{g,BAO}^s(k, \mu_k) = b^2(1 + \beta\mu_k^2)^2 P_{BAO}^{nl}(k, \mu_k)$$

$$= b^2(1 + \beta\mu_k^2)^2 P_{BAO}^{lin}(k) \cdot \exp\left(-\frac{k^2}{2k_*^2}[1 + \mu_k^2(2f + f^2)]\right), \quad (8)$$

Analogous to Eq.(6), the galaxy correlation function can be decomposed into no-wiggle and wiggled parts as follows:

$$\xi_{g,dw}^s(\sigma, \pi) = \xi_{g,nw}^s(\sigma, \pi) + \xi_{g,BAO}^s(\sigma, \pi). \quad (9)$$

While  $\xi_{g,dw}^s(\sigma, \pi)$  can be obtained by Fourier-transforming  $P_g^s(k, \mu_k)$ , doing so involves two-dimensional integrals, and thus is time-consuming and inefficient. Instead, we can Fourier transform each term in Eq.(6) separately, using Legendre polynomial expansions and integral convolutions that only involve one-dimensional integrals.

The no-wiggle galaxy correlation function in redshift space can be computed by Fourier transforming Eq.(7), which gives (Hamilton 1992)

$$\xi_{g,nw}^s(\sigma, \pi) = b^2(\xi_0^{nw}(s)P_0(\mu) + \xi_2^{nw}(s)P_2(\mu) + \xi_4^{nw}(s)P_4(\mu)), \quad (10)$$

where  $s = \sqrt{\sigma^2 + \pi^2}$ ,  $\mu$  is the cosine of the angle between  $\mathbf{s} = (\sigma, \pi)$  and the LOS, and  $P_l$  are Legendre polynomials. The multipoles of  $\xi^{nw}$  are defined as

$$\xi_0^{nw}(r) = \left(1 + \frac{2\beta}{3} + \frac{\beta^2}{5}\right) \xi^{nw}(r), \quad (11)$$

$$\xi_2^{nw}(r) = \left(\frac{4\beta}{3} + \frac{4\beta^2}{7}\right) [\xi^{nw}(r) - \bar{\xi}(r)], \quad (12)$$

$$\xi_4^{nw}(r) = \frac{8\beta^2}{35} \left[\xi^{nw}(r) + \frac{5}{2}\bar{\xi}^{nw}(r) - \frac{7}{2}\bar{\bar{\xi}}^{nw}(r)\right], \quad (13)$$

where  $\beta$  is the linear RSD parameter and

$$\bar{\xi}^{nw}(r) = \frac{3}{r^3} \int_0^r \xi^{nw}(r') r'^2 dr', \quad (14)$$

$$\bar{\bar{\xi}}^{nw}(r) = \frac{5}{r^5} \int_0^r \xi^{nw}(r') r'^4 dr', \quad (15)$$

where  $\xi^{nw}(r)$  is obtained by Fourier transforming  $P_{nw}(k)$ .

The wiggled part of the galaxy correlation function in redshift space,  $\xi_{g,BAO}^s(\sigma, \pi)$ , is obtained by Fourier transforming Eq.(8). Note that the  $\mu$ -dependent damping factor in  $k$ -space in Eq.(8) becomes a Gaussian convolution in configuration space:

$$\xi_{g,BAO}^s(\sigma, \pi) = \int_{-\infty}^{\infty} \xi^*(\sigma, \pi - x) f_*(x) dx, \quad (16)$$

where  $\xi^*(\sigma, \pi)$  is the Fourier transform of  $b^2(1 + \beta\mu_k^2)^2 P_{BAO}^{lin}(k) \cdot \exp(-\frac{k^2}{2k_*^2})$ , and

$$f_*(x) = \frac{1}{\sigma_* \sqrt{\pi}} \exp\left(-\frac{x^2}{\sigma_*^2}\right), \quad (17)$$

where

$$\sigma_*^2 = \frac{4f + 2f^2}{k_*^2}. \quad (18)$$

$\xi^*(\sigma, \pi)$  can be obtained using Eq. (10)-(15), but replace  $\xi^{nw}(r)$  (the Fourier transform of  $P_{nw}(k)$ ) with the Fourier transform of  $P_{BAO}^{lin}(k) \cdot \exp(-\frac{k^2}{2k_*^2})$ .

Table. 1 shows the performance of our convolution method by comparing with the results using fast Fourier transform (FFT) directly. One can see our method is much more efficient. The two-dimensional dewiggle model has a obvious feature at the BAO scale for the normalized quadrupole,  $Q(s)$  (see Samushia et al. 2012, where

box size (Mpc/h) <sup>3</sup>	grid size	computing time (sec)
512 <sup>3</sup>	512 <sup>3</sup>	41
1024 <sup>3</sup>	512 <sup>3</sup>	41
1024 <sup>3</sup>	1024 <sup>3</sup>	352
method used in this study		5

**Table 1.** The time needed for computing the two-dimensional dewiggle model described in Sec. 3.1. We test different methods: one is performing fast Fourier transform (FFT) using FFTW<sup>3</sup> library; the other is the convolution method described in Sec. 3.1 which is the method used in this study. One can see that our method is much faster than FFT method.

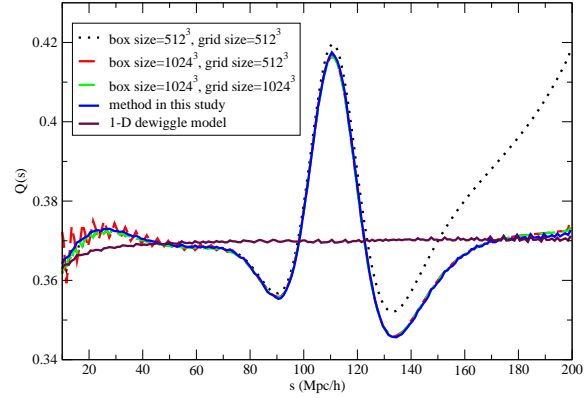


**Figure 1.** The normalized quadrupoles from the correlation functions computed with FFT and our convolution method. One can see that the results from FFT are converging to the result of the convolution method. In addition, FFT method just reaches reasonable convergence with box size = 1024<sup>3</sup> (Mpc/h)<sup>3</sup> and grid size = 1024<sup>3</sup> for the scales considered in this study. One would need to increase the box size or grid size if one want to include other scales. We also plot the  $Q(s)$  from one-dimensional dewiggle model for comparison. It is a constant since the only redshift distortion effect comes from the Kaiser boost.

$$Q(s) = \frac{\xi_2(s)}{\xi_0(s) - (3/s^3) \int_0^s \xi_0(s') s'^2 ds'}. \quad (19)$$

Fig. 1 shows that the results from the FFT method converges to the one from the convolution method. While these tests are performed on a single machine, the grid size used for FFT method is limited by the memory size. One can still see some fluctuations at small scales for the maximum grid size (=1024<sup>3</sup>). Therefore, our method not only provide a much faster way but also use much less resources to compute the theoretical model. With a multi-cores machine (FFT can only use single core unless the machine's memory is much larger), our method could be hundreds times faster than FFT method. It is crucial while doing Markov Chain Monte Carlo (MCMC) analysis.

<sup>3</sup> <http://www.fftw.org/>

### 3.2 Modeling 2D Correlation Function on Small Scales

For small scales, we need to model three effects: the nonlinear matter correlation function, the scale-dependent galaxy bias, and the RSD from the random galaxy pairwise velocities. It is well known that the small scale galaxy correlation function is well described by a powerlaw (Peebles 1980). Since the galaxy correlation function is given by  $\xi^{nw}(r)$  on small scales, we model the combination of nonlinear matter correlation function and the scale-dependent galaxy bias at small scales by multiplying  $\xi^{nw}(r)$  with the following factor

$$b_{nl}(r) = r^{b_A F(r)}, \quad (20)$$

where  $b_A$  is a constant.  $F(r)$  is a function which is close to 1 for small  $r$  and close to 0 when  $r$  is large; we choose

$$F(r) = \frac{1}{1 + \left(\frac{r}{b_B}\right)^{b_C}}, \quad (21)$$

where we choose  $b_B = 30h^{-1}\text{Mpc}$  and  $b_C = 4$ ; these are motivated by the fact that the galaxy correlation function is a powerlaw at small scales (i.e.  $s < 15h^{-1}\text{Mpc}$ ) and the scale-dependent effects (including nonlinear effects and scale-dependent galaxy bias) are negligible at larger scales,  $s > 40h^{-1}\text{Mpc}$ . The overall scale-dependent effects are included when computing the no-wiggle galaxy correlation function by replacing  $\xi^{nw}(r)$  with  $\xi^{nw}(r) \times b_{nl}(r)$  in applying Eq. (10)-(15). The resultant correlation function is denoted as  $\xi_{g,nw}^{s,nl}(\sigma, \pi)$ .

We now obtain the 2D correlation function that incorporate nonlinear effects, galaxy bias, and linear RSD:

$$\tilde{\xi}(\sigma, \pi) = \xi_{g,nw}^{s,nl}(\sigma, \pi) + \xi_{g,BAO}^s(\sigma, \pi), \quad (22)$$

where  $\xi_{g,BAO}^s(\sigma, \pi)$  is given by Eq.(16).

Next, we convolve the 2D correlation function with the distribution function of random pairwise velocities,  $f(v)$ , to obtain the final model  $\xi(\sigma, \pi)$  (Peebles 1980)

$$\xi(\sigma, \pi) = \int_{-\infty}^{\infty} \tilde{\xi}\left(\sigma, \pi - \frac{v}{H(z)a(z)}\right) f(v)dv, \quad (23)$$

where the random motions are represented by an exponential form (Ratcliffe et al. 1998; Landy 2002)

$$f(v) = \frac{1}{\sigma_v(s', \mu'^2)\sqrt{2}} \exp\left(-\frac{\sqrt{2}|v|}{\sigma_v(s', \mu'^2)}\right), \quad (24)$$

where  $\sigma_v$  is the pairwise peculiar velocity dispersion,  $s'^2 = \sigma^2 + \left(\pi - \frac{v}{H(z)a(z)}\right)^2$  and  $\mu' = \frac{1}{s'}\left(\pi - \frac{v}{H(z)a(z)}\right)$ . We find that the 2D correlation functions measured from LasDamas mocks can be well fitted by

$$\sigma_v(s', \mu'^2) = \sigma_{v,0}(1 + C_\mu \mu'^2)(1 + c_{\sigma 1} e^{-c_{\sigma 2} \sigma^2}), \quad (25)$$

where  $\sigma_{v,0}$  is the dispersion corresponding to the truly random motion and  $c_\mu$ ,  $c_{\sigma 1}$ , and  $c_{\sigma 2}$  (with unit of  $\text{Mpc}^{-2}h^2$ ) terms describe the dependence on direction and separation. The  $\sigma$ -dependence is similar to that found by Cabre & Gaztanaga (2009). They found that the 2D correlation functions from the MICE N-body simulations are fitted well with a pairwise velocity distribution which is large when  $\sigma < 5h^{-1}\text{Mpc}$ . We have added the direction-dependent term,  $c_\mu \mu'^2$ , to model the high amplitude of  $\hat{\xi}_4$  at small scales (see Fig. 5).

## 4 METHODOLOGY

In this section, we present the methodology and results of testing our model described in the previous section.

### 4.1 Mock Catalogs Used

We use the 160 mock catalogs from the LasDamas simulations<sup>4</sup> (McBride et al., in preparation) to test our model. LasDamas provides mock catalogs matching SDSS main galaxy and LRG samples. We use the LRG mock catalogs from the LasDamas gamma release with the same cuts as the SDSS LRG DR7full sample,  $-23.2 < M_g < -21.2$  and  $0.16 < z < 0.44$ . We have diluted the mock catalogs to match the radial selection function of the observational data by randomly selecting the mock galaxies according to the number density of the data sample. We calculate the multipoles of the correlation functions of the mock catalogs and construct the covariance matrix (see Chuang & Wang (2013) for details).

### 4.2 Measuring the Two-Dimensional Two-Point Correlation Function

We convert the measured redshifts of galaxies to comoving distances by assuming a fiducial model,  $\Lambda\text{CDM}$  with  $\Omega_m = 0.25$ . We use the two-point correlation function estimator given by Landy & Szalay (1993):

$$\xi(\sigma, \pi) = \frac{DD(\sigma, \pi) - 2DR(\sigma, \pi) + RR(\sigma, \pi)}{RR(\sigma, \pi)}, \quad (26)$$

where  $\pi$  is the separation along the line of sight (LOS),  $\sigma$  is the separation in the plane of the sky, DD, DR, and RR represent the normalized data-data, data-random, and random-random pair counts respectively in a given distance range. The LOS is defined as the direction from the observer to the center of a pair. The bin size we use here is  $1h^{-1}\text{Mpc} \times 1h^{-1}\text{Mpc}$ . The Landy and Szalay estimator has minimal variance for a Poisson process. Random data are generated with the same radial and angular selection functions as the real data. One can reduce the shot noise due to random data by increasing the number of random data. The number of random data we use is 10 times that of the real data. While calculating the pair counts, we assign to each data point a radial weight of  $1/[1 + n(z) \cdot P_w]$ , where  $n(z)$  is the radial selection function and  $P_w = 4 \cdot 10^4 h^{-3}\text{Mpc}^3$  (Eisenstein et al. 2005).

Fig 2 shows the averaged 2D correlation function measured from the mock catalogs. We use the averaged radial selection function to construct the random catalog since it is closer to the true mean density. Clearly, our model provides an excellent fit to data over a wide range of scales, from the largest scales where data are not too noisy, to the smallest scales plotted (except very near the LOS).

### 4.3 Multiples of the Correlation Function

As in Chuang & Wang (2013), the effective multipoles of the correlation function are defined by

$$\hat{\xi}_l(s) \equiv \frac{\sum_{s - \frac{\Delta s}{2} < \sqrt{\sigma^2 + \pi^2} < s + \frac{\Delta s}{2}} (2l + 1)\xi(\sigma, \pi) P_l(\mu) \sqrt{1 - \mu^2}}{\text{Number of bins used in the numerator}}, \quad (27)$$

<sup>4</sup> <http://lss.phy.vanderbilt.edu/lasdama/>

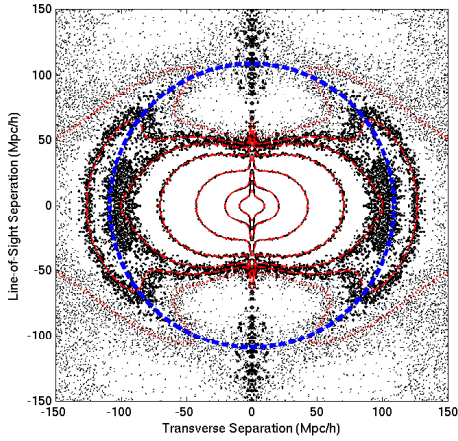


**Figure 2.** The average two-dimensional two-point correlation function (2D 2PCF) measured from 160 LasDamas SDSS LRGfull mock catalogs (solid black contours), compared to a theoretical model with the input parameters of the LasDamas simulations and  $\{\beta, b_A, \sigma_{v,0}, c_\mu, c_\sigma\}$  are set to  $\{0.316, -0.0385, 50\text{km s}^{-1}, 10, 4\}$  (dashed red contours). The thick dashed blue circle denotes the baryon acoustic oscillation scale. The contour levels are  $\xi = 2, 0.5, 0.1, 0.025, 0.01, 0.005, 0$ . The  $\xi = 0$  contours are denoted with dotted lines for clarity.

where  $\Delta s = 5 h^{-1}\text{Mpc}$  in this work, and

$$\sigma = \left(n + \frac{1}{2}\right)h^{-1}\text{Mpc}, n = 0, 1, 2, \dots \quad (28)$$

$$\pi = \left(m + \frac{1}{2}\right)h^{-1}\text{Mpc}, m = 0, 1, 2, \dots \quad (29)$$

$$\mu \equiv \frac{\pi}{\sqrt{\sigma^2 + \pi^2}}. \quad (30)$$

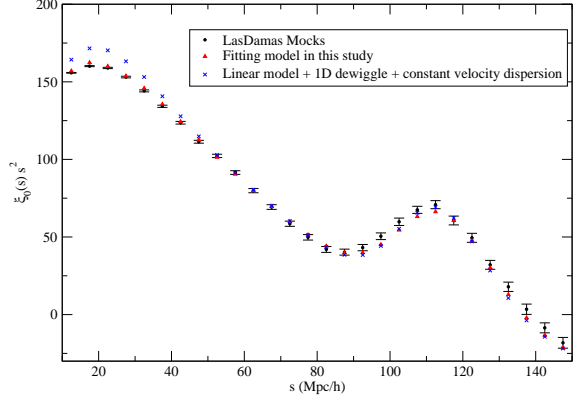
Note that both the measurements and the theoretical predictions for the effective multipoles are computed using Eq.(27). We do not use the conventional definitions of multipoles to extract parameter constraints as they use continuous integrals. Bias could be introduced if the definitions of multipoles are different between measurements from data and the theoretical model.

Fig. 3, 4, and 5 show the effective monopole ( $\hat{\xi}_0$ ), quadrupole ( $\hat{\xi}_2$ ), and hexadecapole ( $\hat{\xi}_4$ ) measured from the LasDamas mock catalogs comparing to our full model and a simpler model (linear model + 1D dewiggle damping + constant velocity dispersion). In Fig. 3, one can see how our model completely corrects the scale-dependent effects in the measured monopole. Fig.4 shows that our model provides a reasonable fit to the measured quadrupole. In Fig. 5, we find that angle-dependent term,  $c_\sigma$ , significantly improves the fitting of hexadecapole at small scales ( $s < 50h^{-1}\text{Mpc}$ ). However, at larger scales ( $s > 60h^{-1}\text{Mpc}$ ), the LasDamas mocks show some oscillatory features while the theoretical models are flat. It is likely due to the dewiggle damping not being adequate enough to model  $\xi_4$  and one might need higher order term (i.e.  $\mu^4$ ). Therefore, we do not include  $\xi_4$  to measure parameters in this study.

#### 4.4 Covariance Matrix

We construct the covariance matrix as

$$C_{ij} = \frac{1}{N-1} \sum_{k=1}^N (\bar{X}_i - X_i^k)(\bar{X}_j - X_j^k), \quad (31)$$



**Figure 3.** The averaged monopole of the correlation functions of the mock catalogs (black squares) comparing to the fitting model of this study (red dots) and a simpler model (linear model + 1D dewiggle damping + constant velocity dispersion, blue crosses). The error bars are taken as  $1/\sqrt{160}$  of the square roots of the diagonal elements of the covariance matrix.

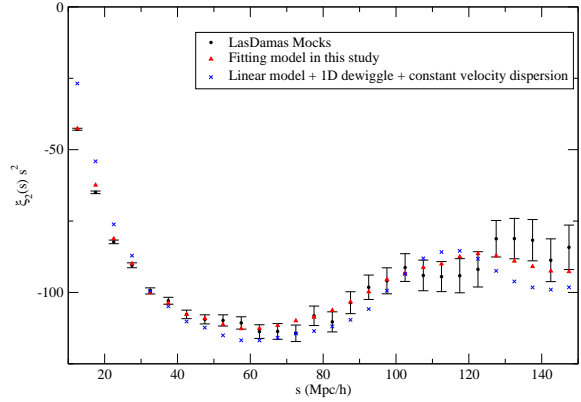


**Figure 4.** The averaged quadrupole of the correlation functions of the mock catalogs (black squares) comparing to the fitting model of this study (red dots) and a simpler model (linear model + 1D dewiggle damping + constant velocity dispersion, blue crosses). The error bars are taken as  $1/\sqrt{160}$  of the square roots of the diagonal elements of the covariance matrix.

where  $N$  is the number of the mock catalogs,  $\bar{X}_m$  is the mean of the  $m^{\text{th}}$  element of the vector from the mock catalog multipoles, and  $X_m^k$  is the value in the  $m^{\text{th}}$  elements of the vector from the  $k^{\text{th}}$  mock catalog multipoles. The data vector  $\mathbf{X}$  is defined by

$$\mathbf{X} = \{\hat{\xi}_0^{(1)}, \hat{\xi}_0^{(2)}, \dots, \hat{\xi}_0^{(N)}; \hat{\xi}_2^{(1)}, \hat{\xi}_2^{(2)}, \dots, \hat{\xi}_2^{(N)}; \dots\}, \quad (32)$$

where  $N$  is the number of data points in each measured multipole;  $N = 19$  while using the scale range,  $25 < s < 120h^{-1}\text{Mpc}$ . The length of the data vector  $\mathbf{X}$  depends on how many multipoles are used.

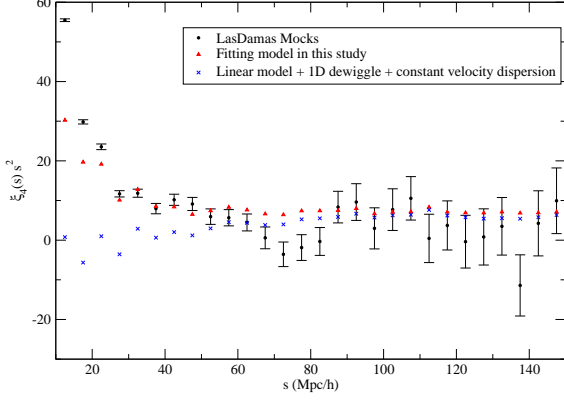


**Figure 5.** The averaged hexadecapole of the correlation functions of the mock catalogs (black squares) comparing to the fitting model of this study (red dots) and a simpler model (linear model + 1D dewiggle damping + constant velocity dispersion, blue crosses). The error bars are taken as  $1/\sqrt{160}$  of the square roots of the diagonal elements of the covariance matrix.

#### 4.5 Likelihood

The likelihood is taken to be proportional to  $\exp(-\chi^2/2)$  (Press et al. 1992), with  $\chi^2$  given by

$$\chi^2 \equiv \sum_{i,j=1}^{N_X} [X_{th,i} - X_{obs,i}] C_{ij}^{-1} [X_{th,j} - X_{obs,j}] \quad (33)$$

where  $N_X$  is the length of the vector used,  $X_{th}$  is the vector from the theoretical model, and  $X_{obs}$  is the vector from the observational data (we use the mock catalogs as the observational data to test the model in this section).

As explained in Chuang & Wang (2012), instead of recalculating the observed correlation function for different theoretical models, we rescale the theoretical correlation function to avoid rendering  $\chi^2$  values arbitrary. The rescaled theoretical correlation function is computed by

$$T^{-1}(\xi_{th}(\sigma, \pi)) = \xi_{th} \left( \frac{D_A(z)}{D_A^{fid}(z)} \sigma, \frac{H^{fid}(z)}{H(z)} \pi \right), \quad (34)$$

where  $\xi_{th}$  is given by eq. (23). Hence  $\chi^2$  can be rewritten as

$$\chi^2 \equiv \sum_{i,j=1}^{N_X} \left\{ T^{-1} X_{th,i} - X_{obs,i}^{fid} \right\} C_{fid,ij}^{-1} \cdot \left\{ T^{-1} X_{th,j} - X_{obs,j}^{fid} \right\}, \quad (35)$$

where  $T^{-1} X_{th}$  is a vector given by eq. (34) with  $\xi_{th}$  replaced by its effective multipoles (defined by eq. (27)), and  $X_{obs}^{fid}$  is the corresponding vector from observational data measured assuming the fiducial model in converting redshifts to distances. See Chuang & Wang (2012) for a more detailed description of our rescaling method.

#### 4.6 Markov Chain Monte-Carlo Likelihood Analysis

We use CosmoMC in a Markov Chain Monte-Carlo likelihood analysis (Lewis & Bridle 2002). The parameter space that we explore spans the parameter set of  $\{H(0.35), D_A(0.35), \Omega_m h^2,$

	$25 < s < 120$	input value
$H(0.35)$	$82.8 \pm 11$	81.79
$D_A(0.35)$	$1023 \pm 77$	1032.8
$\Omega_m h^2$	$0.120 \pm 0.020$	0.1225
$H(0.35) r_s(z_d)/c$	$0.0444 \pm 0.0054$	0.0434
$D_A(0.35)/r_s(z_d)$	$6.35 \pm 0.45$	6.48
$f(0.35) * \sigma_8(0.35)$	$0.445 \pm 0.097$	0.437

**Table 2.** The mean and standard deviation of  $\{H(0.35), D_A(0.35), \Omega_m h^2, H(0.35) r_s(z_d)/c, D_A(0.35)/r_s(z_d), f(0.35) \sigma_8(0.35)\}$  from the averaged correlation function from LasDamas SDSS LRG mock catalogs using  $\hat{\xi}_0 + \hat{\xi}_2$  and the scale range,  $25 < s < 120 h^{-1} \text{Mpc}$ , comparing with the input values of the simulations. One can see that the input values of the simulations are well recovered by our methodology. The unit of  $H$  is  $\text{km s}^{-1} \text{Mpc}^{-1}$ . The unit of  $D_A$  and  $r_s(z_d)$  is Mpc.

$\beta, b\sigma_8(z), \Omega_b h^2, n_s, k_*, f(0.35), b_A, \sigma_{v,0}, c_\mu, c_{\sigma 1}, c_{\sigma 2}\}$ . Only  $\{H(0.35), D_A(0.35), \Omega_m h^2, \beta, b\sigma_8(z)\}$  are well constrained by the mock data.

We marginalize over the other parameters,  $\{\Omega_b h^2, n_s, k_*, f(0.35), b_A, \sigma_{v,0}, c_\mu, c_{\sigma 1}, c_{\sigma 2}\}$ , with flat priors over the ranges of  $\{(0.01859, 0.02657), (0.865, 1.059), (0.09, 0.15) \text{Mpc}^{-1} h, (0.3, 1.0), (-0.2, 0.2), (0, 500) \text{s}^{-1} \text{km}, (0, 20), (0, 10), (0.01, 0.2) \text{Mpc}^{-2} h^2\}$ , where the flat priors of  $\Omega_b h^2$  and  $n_s$  are centered on the measurements from WMAP7 and has width of  $\pm 7\sigma_{WMAP}$  (with  $\sigma_{WMAP}$  from Komatsu et al. (2010)). These priors are wide enough to ensure that CMB constraints are not double counted when our results are combined with CMB data (Chuang, Wang, & Hemantha 2012).

#### 4.7 Validation of the Model Using Mock catalogs

We apply our method on the averaged correlation function from LasDamas SDSS LRG mock catalogs to validate our methodology. Table 2 shows the measurements of  $\{H(0.35), D_A(0.35), \Omega_m h^2, H(0.35) r_s(z_d)/c, D_A(0.35)/r_s(z_d), f(0.35) \sigma_8(0.35)\}$  from the averaged correlation function from LasDamas SDSS LRG mock catalogs using  $\hat{\xi}_0 + \hat{\xi}_2$  and the scale range,  $25 < s < 120 h^{-1} \text{Mpc}$ , comparing with the input values of the simulations. We find the input values of the simulations are well recovered by our methodology.

### 5 MEASUREMENTS FROM SDSS DR7 LRG

Table 3 lists the mean and rms variance of the parameters,  $\{H(0.35), D_A(0.35), \Omega_m h^2, \beta, b\sigma_8(z), H(0.35) r_s(z_d)/c, D_A(0.35)/r_s(z_d), f(z) \sigma_8(z)\}$ , derived in an MCMC likelihood analysis from the measured  $\hat{\xi}_0 + \hat{\xi}_2$  of the correlation function of the SDSS LRG sample with the scale range,  $25 < s < 120 h^{-1} \text{Mpc}$  and  $40 < s < 120 h^{-1} \text{Mpc}$ . Table 4 and 5 gives the corresponding normalized covariance matrices.

While we are modeling the correlation function on small scales, the uncertainties would still become larger when smaller scales are included. Although one could obtain tighter constraints by using very small scales, to be conservative, we only fit the measurements using scales larger than  $25 h^{-1} \text{Mpc}$  and check the consistency with the measurements using the scales larger than  $40 h^{-1} \text{Mpc}$ .

Our measurements are consistent between two scale ranges

	$25 < s < 120$	$40 < s < 120$
$H(0.35)$	$82.7 \pm 8.4$	$79 \pm 12$
$D_A(0.35)$	$1036 \pm 79$	$1039 \pm 113$
$\Omega_m h^2$	$0.1226 \pm 0.025$	$0.101 \pm 0.017$
$\beta$	$0.388 \pm 0.081$	$0.426 \pm 0.15$
$b\sigma_8(z)$	$1.110 \pm 0.079$	$1.038 \pm 0.095$
$H(0.35)r_s(z_d)/c$	$0.0433 \pm 0.0042$	$0.0432 \pm 0.0064$
$D_A(0.35)/r_s(z_d)$	$6.59 \pm 0.46$	$6.30 \pm 0.65$
$f(0.35)\sigma_8(0.35)$	$0.429 \pm 0.089$	$0.438 \pm 0.14$
$\chi^2/\text{d.o.f.}$	$1.07 - 1.46$	$1.05 - 1.57$

**Table 3.** The mean and standard deviation of  $\{H(0.35), D_A(0.35), \Omega_m h^2, \beta, b\sigma_8(z), H(0.35)r_s(z_d)/c, D_A(0.35)/r_s(z_d), f(0.35)\sigma_8(0.35)\}$  from SDSS DR7 LRGs using  $\xi_0 + \hat{\xi}_2$  and the scale ranges,  $25 < s < 120h^{-1}\text{Mpc}$  and  $40 < s < 120h^{-1}\text{Mpc}$ . We report the minimum and maximum  $\chi^2$  per degree of freedom since there are many fitting parameters are not well constrained. The unit of  $H$  is  $\text{km s}^{-1} \text{Mpc}^{-1}$ . The unit of  $D_A$  and  $r_s(z_d)$  is Mpc.

considered which shows no hint of systematics. We choose the results using the scale range,  $25 < s < 120h^{-1}\text{Mpc}$ , as our fiducial results. As expected, the constraints become tighter when including smaller scales. Notice that the correlations between  $\Omega_m h^2$  and  $\{H(0.35)r_s(z_d)/c, D_A(0.35)/r_s(z_d)\}$  also increase. It is due to the fact that our measurements gain more constraining power from the overall shape beyond the BAO peak region.

## 6 CONCLUSION AND DISCUSSION

We have presented and validated a simple and efficient phenomenological model for the two-dimensional two-point galaxy correlation function that works well over a wide range of scales, from large scales down to small scales not used in our previous work (where we restricted ourselves to scales larger than  $40h^{-1}\text{Mpc}$ ). Applying this model to the SDSS LRGs over the scale range of  $25 < s < 120h^{-1}\text{Mpc}$ , We obtain the measurements:  $H(z)r_s(z_d)/c = 0.0433 \pm 0.0042$ ,  $D_A(z)/r_s(z_d) = 6.59 \pm 0.46$ , and  $f(z)\sigma_8(z) = 0.429 \pm 0.089$  at  $z = 0.35$ , which summarize the cosmological constraints extracted from the SDSS DR7 LRG sample. We also provide the covariance matrix needed to use these measurements (see Table 4).

Our model incorporates the overall nonlinear effects via the use of the ‘‘dewiggled’’ galaxy power spectrum, as in Chuang & Wang (2012), but we now include the enhanced damping along the line of sight (see Eqs.(1)-(4)). We also introduce a much efficient way to compute this model which is crucial for MCMC analysis. On small scales, the nonlinear effect and scale-dependent galaxy bias are degenerate, and we model these as an overall scale-dependent correction. Most significantly, we allow the RSD to be scale and direction dependent in our model. Our model provides excellent fit to mock data (see Fig.2).

We expect our methodology and results to be useful in tightening dark energy and gravity constraints from the full analysis of current and future galaxy clustering data.

## ACKNOWLEDGEMENTS

We are grateful to the LasDamas project for making their mock catalogs publicly available. The computing for this project was performed at the OU Supercomputing Center for Education and Research (OSCAR) at the University of Oklahoma (OU). This work used the Extreme Science and Engineering Discovery Environment (XSEDE), which is supported by National Science Foundation grant number OCI-1053575. This work was supported by DOE grant DE-FG02-04ER41305. C.C. was also supported by the Spanish MICINN’s Consolider-Ingenio 2010 Programme under grant MultiDark CSD2009-00064 and grant AYA2010-21231, the Comunidad de Madrid under grant HEPHACOS S2009/ESP-1473, and the Spanish MINECO’s Centro de Excelencia Severo Ochoa Programme under grant SEV-2012-0249.

Funding for the Sloan Digital Sky Survey (SDSS) has been provided by the Alfred P. Sloan Foundation, the Participating Institutions, the National Aeronautics and Space Administration, the National Science Foundation, the U.S. Department of Energy, the Japanese Monbukagakusho, and the Max Planck Society. The SDSS Web site is <http://www.sdss.org/>.

The SDSS is managed by the Astrophysical Research Consortium (ARC) for the Participating Institutions. The Participating Institutions are The University of Chicago, Fermilab, the Institute for Advanced Study, the Japan Participation Group, The Johns Hopkins University, Los Alamos National Laboratory, the Max-Planck-Institute for Astronomy (MPIA), the Max-Planck-Institute for Astrophysics (MPA), New Mexico State University, University of Pittsburgh, Princeton University, the United States Naval Observatory, and the University of Washington.

## REFERENCES

- Abazajian, K. N., *et al.* [SDSS Collaboration], *Astrophys. J. Suppl.* **182**, 543 (2009) [arXiv:0812.0649 [astro-ph]].
- Anderson, L., *et al.*, arXiv:1303.4666 [astro-ph.CO].
- Blake, C., Glazebrook, K., 2003, *ApJ*, 594, 665
- Blake, C.; Collister, A.; Bridle, S.; and Lahav, O., *Mon. Not. Roy. Astron. Soc.* **374**, 1527 (2007) [arXiv:astro-ph/0605303].
- Blake, C., *et al.* 2009, *MNRAS*, 395, 240
- Blanton, M. R., *et al.* [SDSS Collaboration], *Astron. J.* **129**, 2562 (2005) [arXiv:astro-ph/0410166].
- Blanton, M. R.; and Roweis, S., *Astron. J.* **133**, 734 (2007) [arXiv:astro-ph/0606170].
- Cabre, A.; and Gaztanaga, E., *Mon. Not. Roy. Astron. Soc.* **393**, 1183 (2009) [arXiv:0807.2460 [astro-ph]].
- Chuang, C. -H.; Wang, Y.; and Hemantha, M. D. P., *Mon. Not. Roy. Astron. Soc.* **423**, 1474 (2012) [arXiv:1008.4822 [astro-ph.CO]].
- Chuang, C. -H. and Wang, Y. *Mon. Not. Roy. Astron. Soc.* **426**, 226 (2012) [arXiv:1102.2251 [astro-ph.CO]].
- Chuang, C. -H. and Wang, Y. *Mon. Not. Roy. Astron. Soc.* **431**, 2634 (2013) [arXiv:1205.5573 [astro-ph.CO]].
- Chuang, C. -H., *et al.*, arXiv:1303.4486 [astro-ph.CO].
- Cimatti, A., *et al.*, *Exper. Astron.* **23**, 39 (2009) [arXiv:0804.4433 [astro-ph]].
- Crocce, M., and Scoccimarro, R., *Phys. Rev. D* **73**, 063520 (2006) [arXiv:astro-ph/0509419].
- Eisenstein, D. J.; and Hu, W., *Astrophys. J.* **496**, 605 (1998) [arXiv:astro-ph/9709112].
- Eisenstein, D. J., *et al.* [SDSS Collaboration], *Astron. J.* **122**, 2267 (2001) [arXiv:astro-ph/0108153].

	$H(0.35)$	$D_A(0.35)$	$\Omega_m h^2$	$\beta$	$b\sigma_8(0.35)$	$H(0.35) r_s(z_d)/c$	$D_A(0.35)/r_s(z_d)$	$f(0.35)\sigma_8(0.35)$
$H(0.35)$	1.0000	-0.0069	0.3361	0.4316	-0.0867	0.8478	0.2602	0.3995
$D_A(0.35)$	-0.0069	1.0000	-0.4422	0.2151	-0.0338	0.2539	0.7257	0.2029
$\Omega_m h^2$	0.3361	-0.4422	1.0000	0.1189	0.6116	-0.1937	0.2664	0.3278
$\beta$	0.4316	0.2151	0.1189	1.0000	-0.1693	0.3983	0.3011	0.9400
$b\sigma_8(0.35)$	-0.0867	-0.0338	0.6116	-0.1693	1.0000	-0.3864	0.3746	0.1705
$H(0.35) r_s(z_d)/c$	0.8478	0.2539	-0.1937	0.3983	-0.3864	1.0000	0.1195	0.2626
$D_A(0.35)/r_s(z_d)$	0.2602	0.7257	0.2664	0.3011	0.3746	0.1195	1.0000	0.4299
$f(0.35)\sigma_8(0.35)$	0.3995	0.2029	0.3278	0.9400	0.1705	0.2626	0.4299	1.0000

**Table 4.** Normalized covariance matrix of the measured and derived parameters,  $\{H(0.35), D_A(0.35), \Omega_m h^2, \beta, b\sigma_8(0.35), H(0.35) r_s(z_d)/c, D_A(0.35)/r_s(z_d), f(0.35)\sigma_8(0.35)\}$  from SDSS DR7 LRGs using  $\hat{\xi}_0 + \hat{\xi}_2$  and the scale range,  $25 < s < 120h^{-1}\text{Mpc}$ .

	$H(0.35)$	$D_A(0.35)$	$\Omega_m h^2$	$\beta$	$b\sigma_8(0.35)$	$H(0.35) r_s(z_d)/c$	$D_A(0.35)/r_s(z_d)$	$f(0.35)\sigma_8(0.35)$
$H(0.35)$	1.0000	0.1050	0.2602	0.4394	-0.1514	0.9566	0.2280	0.4217
$D_A(0.35)$	0.1050	1.0000	-0.2925	0.3573	0.1515	0.2001	0.9164	0.4097
$\Omega_m h^2$	0.2602	-0.2925	1.0000	-0.0115	0.5157	-0.0164	0.0903	0.1284
$\beta$	0.4394	0.3573	-0.0115	1.0000	-0.2872	0.4593	0.3711	0.9627
$b\sigma_8(0.35)$	-0.1514	0.1515	0.5157	-0.2872	1.0000	-0.2911	0.3396	-0.0357
$H(0.35) r_s(z_d)/c$	0.9566	0.2001	-0.0164	0.4593	-0.2911	1.0000	0.2068	0.4037
$D_A(0.35)/r_s(z_d)$	0.2280	0.9164	0.0903	0.3711	0.3396	0.2068	1.0000	0.4758
$f(0.35)\sigma_8(0.35)$	0.4217	0.4097	0.1284	0.9627	-0.0357	0.4037	0.4758	1.0000

**Table 5.** Normalized covariance matrix of the measured and derived parameters,  $\{H(0.35), D_A(0.35), \Omega_m h^2, \beta, b\sigma_8(0.35), H(0.35) r_s(z_d)/c, D_A(0.35)/r_s(z_d), f(0.35)\sigma_8(0.35)\}$  from SDSS DR7 LRGs using  $\hat{\xi}_0 + \hat{\xi}_2$  and the scale range,  $40 < s < 120h^{-1}\text{Mpc}$ .

- Eisenstein, D. J., *et al.* [SDSS Collaboration], *Astrophys. J.* **633**, 560 (2005) [arXiv:astro-ph/0501171].
- D. J. Eisenstein, H. -j. Seo and M. J. White, 1, *Astrophys. J.* **664**, 660 (2007) [astro-ph/0604361].
- Eisenstein, D.J., *et al.*, 2011, *AJ*, 142, 72
- Fukugita, M.; Ichikawa, T.; Gunn, J. E.; Doi, M.; Shimasaku, K.; and Schneider, D. P., *Astron. J.* **111**, 1748 (1996).
- Gunn, J. E., *et al.* [SDSS Collaboration], *Astron. J.* **116**, 3040 (1998) [arXiv:astro-ph/9809085].
- Gunn, J. E., *et al.* [SDSS Collaboration], *Astron. J.* **131**, 2332 (2006) [arXiv:astro-ph/0602326].
- Guzzo, L., *et al.*, 2008, *Nature*, 451, 541
- Hamilton, A. J. S., 1992, *APJL*, 385, L5
- Hutsi, G., arXiv:astro-ph/0507678.
- Jennings, E.; Baugh, C. M.; and Pascoli, S., *Mon. Not. Roy. Astron. Soc.* **410**, 2081 (2011) [arXiv:1003.4282 [astro-ph.CO]].
- Kaiser, N., *Mon. Not. Roy. Astron. Soc.* **227**, 1 (1987).
- Kazin, E. A., *et al.*, *Astrophys. J.* **710**, 1444 (2010) [arXiv:0908.2598 [astro-ph.CO]].
- Kazin, E. A.; Blanton, M. R.; Scoccimarro, R.; McBride, C. K.; and Berlind, A. A., *Astrophys. J.* **719**, 1032 (2010) [arXiv:1004.2244 [astro-ph.CO]].
- Komatsu, E. *et al.* [WMAP Collaboration], *Astrophys. J. Suppl.* **192**, 18 (2011) [arXiv:1001.4538 [astro-ph.CO]].
- Landy, S. D. and Szalay, A. S., *Astrophys. J.* **412**, 64 (1993).
- Landy, S. D., “The Pairwise Velocity Distribution Function of Galaxies in the LCRS, 2dF, *Astrophys. J.* **567**, L1 (2002) [arXiv:astro-ph/0202130].
- Laureijs, R., *et al.*, “Euclid Definition Study Report”, arXiv:1110.3193
- Lewis, A.; Challinor, A.; and Lasenby, A., *Astrophys. J.* **538**, 473 (2000) [arXiv:astro-ph/9911177].
- Lewis, A. and Bridle, S., *Phys. Rev. D* **66**, 103511 (2002) [arXiv:astro-ph/0205436].
- Martinez, V. J., *et al.*, *Astrophys. J.* **696**, L93 (2009) [Erratum-ibid. **703**, L184 (2009)] [*Astrophys. J.* **703**, L184 (2009)] [arXiv:0812.2154 [astro-ph]].
- Matsubara, T., *Phys. Rev. D* **77**, 063530 (2008) [arXiv:0711.2521 [astro-ph]].
- Montesano, F.; Sanchez, A. G.; and Phleps, S., arXiv:1107.4097 [astro-ph.CO].
- Okumura, T.; Matsubara, T.; Eisenstein, D. J.; Kayo, I.; Hikage, C.; Szalay, A. S.; and Schneider, D. P., *Astrophys. J.* **676**, 889 (2008) [arXiv:0711.3640 [astro-ph]].
- Padmanabhan, N., *et al.* [SDSS Collaboration], *Mon. Not. Roy. Astron. Soc.* **378**, 852 (2007) [arXiv:astro-ph/0605302].
- Padmanabhan, N.; Xu, X.; Eisenstein, D. J.; Scalzo, R.; Cuesta, A. J.; Mehta, K. T.; and Kazin, E., arXiv:1202.0090 [astro-ph.CO].
- Peebles, P. J. E. 1980, *The Large-Scale Structure of the Universe* (Princeton, NJ: Princeton University Press)
- Percival, W. J.; Cole, S.; Eisenstein, D. J.; Nichol, R. C.; Peacock, J. A.; Pope, A. C.; and Szalay, A. S., *Mon. Not. Roy. Astron. Soc.* **381**, 1053 (2007) [arXiv:0705.3323 [astro-ph]].
- Percival, W. J., *et al.*, *Mon. Not. Roy. Astron. Soc.* **401**, 2148 (2010) [arXiv:0907.1660 [astro-ph.CO]].
- Perlmutter, S., *et al.* [Supernova Cosmology Project Collaboration], *Astrophys. J.* **517**, 565 (1999) [arXiv:astro-ph/9812133].
- Press W.H., Teukolsky S.A., Vetterling W.T., Flannery B.P., 1992, *Numerical recipes in C. The art of scientific computing*, Second edition, Cambridge: University Press.
- Ratcliffe, A., *et al.*, 1998, *VizieR Online Data Catalog*, 730, 417
- Reid, B. A., *et al.*, *Mon. Not. Roy. Astron. Soc.* **404**, 60 (2010)

- [arXiv:0907.1659 [astro-ph.CO]].
- Reid, B. A.; and White, M., Mon. Not. Roy. Astron. Soc. **417**, 1913 (2011) [arXiv:1105.4165 [astro-ph.CO]].
- Reid, B.A., et al. Mon. Not. Roy. Astron. Soc. **426**, 2719 (2012) [arXiv:1203.6641].
- Riess, A. G., *et al.* [Supernova Search Team Collaboration], Astron. J. **116**, 1009 (1998) [arXiv:astro-ph/9805201].
- Sanchez, A. G.; Crocce, M.; Cabre, A.; Baugh, C. M.; and Gaztanaga, E., arXiv:0901.2570 [astro-ph].
- Samushia, L.; Percival, W. J.; and Raccanelli, A., Mon. Not. Roy. Astron. Soc. **420**, 2102 (2012) [arXiv:1102.1014 [astro-ph.CO]].
- Seo, H., Eisenstein, D. J., 2003, ApJ, 598, 720
- Song, Y.-S.; Percival, W. J., 2009, JCAP, 10, 004
- Tegmark, M., *et al.* [SDSS Collaboration], Astrophys. J. **606**, 702 (2004) [arXiv:astro-ph/0310725].
- Wang, Y., 2006, ApJ, 647, 1
- Wang, Y., 2008, JCAP, 05, 021
- Wang, Y., et al., MNRAS, 409, 737 (2010)
- Wang, Y., 2012, MNRAS, 423, 3631
- Wang, Y.; Chuang, C. -H.; and Mukherjee, P., Phys. Rev. D **85**, 023517 (2012) [arXiv:1109.3172 [astro-ph.CO]].
- Xu, X.; Cuesta, A. J.; Padmanabhan, N.; Eisenstein, D. J.; and McBride, C. K., Mon. Not. Roy. Astron. Soc. **431**, 2834 (2013) [arXiv:1206.6732 [astro-ph.CO]].
- Zehavi, I., *et al.* [SDSS Collaboration], Astrophys. J. **621**, 22 (2005) [arXiv:astro-ph/0411557].